ELSEVIER

Spectrochimica Acta Part A 56 (2000) 1051–1064

SPECTROCHIMICA ACTA PART A

www.elsevier.nl/locate/saa

Structural and vibrational characterisation of 3-amino-1-propanol a concerted SCF-MO ab initio, Raman and infrared (matrix isolation and liquid phase) spectroscopy study

Constança Cacela [a], M.L. Duarte [a], Rui Fausto [b,*]

[a] *Departamento de Química e Bioquímica, CECUL, Faculdade de Ciências, Universidade de Lisboa, 1749-016 Lisbon, Portugal*
[b] *Departamento de Química, Universidade de Coimbra, P-3049 Coimbra, Portugal*

Received 20 July 1999; accepted 31 August 1999

Abstract

Results obtained for the isolated and liquid 3-amino-1-propanol by a concerted molecular orbital and vibrational spectroscopic approach are reported. The relative energies and both structural and vibrational data of the different conformers of the studied compound were calculated using the extended 6-31G* basis set both at the HF-SCF and MP2 ab initio levels of theory and the theoretical results used to interpret Raman and infrared experimental data. In the gaseous phase and for the molecule isolated in an Argon matrix, monomeric 3-amino-1-propanol exists as a mixture of conformers, the first and second lowest energy forms corresponding to conformers which exhibit an intramolecular OH–N hydrogen bond (forms I and II). On the other hand, in the pure liquid, where intermolecular H-bonding occurs, the monomeric unit within the aggregates assumes a conformation similar to that of the third most stable form found for the isolated molecule situation (form III), which is characterised by having a weak intramolecular NH–O bond. The experimental data obtained for the pure liquid also reveals the presence of monomeric form I in this phase, a result that is in consonance with the strongly stabilizing OH–N intramolecular hydrogen bond that is present in this conformer.

Keywords: 3-Amino-1-propanol; Intra and intermolecular hydrogen bonding; Infrared and Raman spectra; Matrix isolation; HF-SCF; MP2 6-31G* ab initio calculations

1. Introduction

The conformational isomerism in isolated and liquid 2-aminoethanol (2AE) has been recently investigated in our laboratory by a concerted molecular orbital and vibrational spectroscopic approach [1]. In the present study, results ob-

* Corresponding author. Tel.: +351-39-22826; fax: +351-39-27703.
E-mail address: rfausto@gemini.ci.uc.pt (R. Fausto)

1386-1425/00/$ - see front matter
PII: S1386-1425(99)00203-6

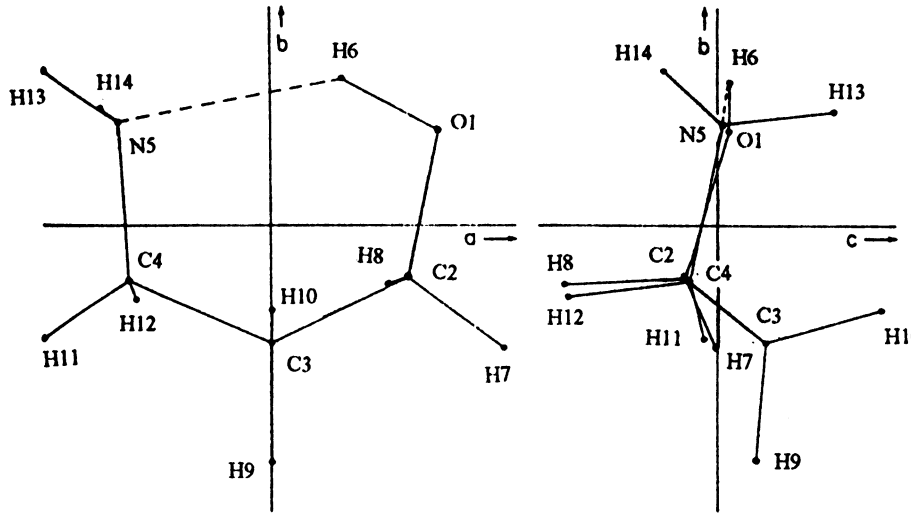

Fig. 1. Projections of the resulting structure of 3-amino-1-propanol obtained by microwave spectroscopy (adapted from [2]).

tained for the more complex aminoalcohol 3-amino-1-propanol (3AP) using a similar methodology are reported.

From our previous studies in 2AE, it could be established that the simultaneous presence in this molecule of the NH_2 and OH groups allows the establishment of different types of intra and intermolecular hydrogen bonding which were found to have different importance in the various phases studied. For the isolated molecule, OH–N and NH–O intramolecular hydrogen bonding may occur, the first being considerably stronger than the last [1]. On the other hand, in the liquid phase, the intramolecular NH–O hydrogen bonding plays a prominent role in stabilising the conformations that are the most populated forms under this condition, while the OH–N intramolecular hydrogen bonding is virtually absent. This latter is replaced by the stronger OH–N intermolecular hydrogen bonding that becomes the prevalent interaction in this phase [1]. In a similar way to that found in 2AE, it can than be expected that, both in isolated and liquid 3AP, hydrogen bonding interactions are also the main factor leading to the stabilisation of certain conformations.

3AP is characterised by four independent torsional angles (lp-N5-C4-C3, N5-C4-C3-C2, C4-C3-C2-O1, C3-C2-O1-H6; lp, lone pair). The different stable conformations are obtained by rotation around the C4N5, C3C4, C2C3 and O1C2 bonds, and the values of the appropriate dihedral angles are, in all cases, expected to be close to 60°, −60° and 180°.

In a microwave study of 3AP [2] in the gaseous phase, a structure close to a gauche-gauche-gauche-gauche form, with an OH–N intramolecular hydrogen bond, was found to be the most stable conformer (Fig. 1). To simultaneously form the hydrogen bond and keep the internal rotation energy minimum, the molecule folded itself to a compact six-membered ring, the OCCCN framework being slightly distorted from the exactly staggered configuration towards planarity. A recent gas-phase infrared study supported the microwave results, clearly demonstrating that a conformer with an intramolecular OH–N bond strongly predominates in this phase, while evidences of the presence of a second conformer with a free OH group were also presented [3].

Theoretical studies carried out at the HF 4-31G [4–6] and DFT B3lyp [3] levels have also established the importance of the intramolecular OH–N interaction in this type of compounds. For 3AP, these calculations indicate that this interaction is present in the two most stable conformations, despite in the second lowest energy form it is of minor importance. The intramolecular NH–O interaction was considered to be present in

four of the minima found in the potential energy surface of 3AP, but it was suggested to be a weak interaction [3–6].

In an infrared spectroscopic study of aminoalcohols in solution [7] it was proposed that the presence in these compounds of strong intramolecular hydrogen bonding may reduce considerably their association tendency, so that a considerable amount of intramolecularly hydrogen-bonded species may exist in concentrated solutions. The associated species formed were largely composed of cyclic dimers, whose precise nature was found to depend on the strength of the intramolecular hydrogen bond. In 3AP, the dimers involved the participation of the nitrogen atom, so that fairly large ring dimers (twelve-membered), with an intermolecular OH–N hydrogen bond, are formed [7].

As mentioned above, the prevalent hydrogen bonding in liquid 2AE is the intermolecular OH–N bonding [1]. The formation of this bond, whose mean energy of stabilization is known to be ca. 29 kJ mol^{-1} [8] (i.e. nearly twice that associated with the intramolecular process in the most stable conformer [1,9]), leads necessarily to the break of the intramolecular OH–N hydrogen bond of the two most stable forms found in the vapour phase. Indeed, no spectroscopic evidence of the presence of these two forms in liquid 2AE could be found [1]. The preferred conformations in the liquid phase are those which have an intramolecular NH–O hydrogen bond, that was found to activate both the OH and NH_2 groups to the establishment of the prevalent OH–N intermolecular hydrogen bond. It could be expected that 3AP should show a similar behaviour. Nevertheless, since 3AP has an increased conformational flexibility (which shall lead to stronger intramolecular hydrogen bonding), its association tendency shall reduce when compared to 2AE, and we would expect an increased amount of the free intramolecularly OH–N hydrogen bonded species to be present in the pure liquid. Such hypothesis appeared attractive to investigation, since the relative amount of free versus associated species may play a dominant role in determining the ability of linear aminoalcohols to form very stable glasses that can be successfully used to prevent ice formation during the process of vitrification in organ or biological tissues cryopreservation [10]. In addition, to date, most of the theoretical studies on 3AP have focused only on the energies, structures and intramolecular interactions of the most stable conformations for the isolated molecule situation. The vibrational data is very scarce and have not yet been correlated with a high level theoretical model.

In this article, the vibrational spectra of 3AP in the liquid phase, in CCl_4 solution and isolated in an Ar matrix are presented. These data are interpreted with the help of theoretical results obtained from vibrational calculations carried out using the HF/SCF-MO 6–31G* ab initio calculated force fields.

2. Experimental

3AP was obtained commercially spectroscopic grade (Aldrich, purity 99 + %) and was used without any additional purification. The sample was handled in a glove box to avoid moisture from air. To undertake the matrix-isolation infrared studies the sample was pre-mixed with Ar (99,999% purity) under reduced pressure. The gas mixture (matrix:solute = 1500) thus formed was then sprayed onto the cold KBr window at 14 K. The gas flux was controlled with two swagelok valves (models BMG and BMRG), which make the connection to an APD cryogenics DMX closed cycle helium refrigeration system whose principal component is a DE-202 Displex expander. The refrigeration system is supported by an APD cryogenics Helium compressor (model HC-2D-1). For the conventional IR spectra a specially designed demountable transmission variable temperature cell with KBr windows, linked to a T48 (Red Lion Controls) temperature controller was used. The IR spectra were obtained using a Mattson (Infinity Series) or a Bomem (MB104) Fourier Transformer spectrometer equipped with a deuterated triglycine sulphide (DTGS) detector and Ge/KBr or Zn/Se optics. Data collection was performed with 1 cm^{-1} spectral resolution. Solution studies were undertaken at room temperature using CCl_4 (Riedel-de-Häen,

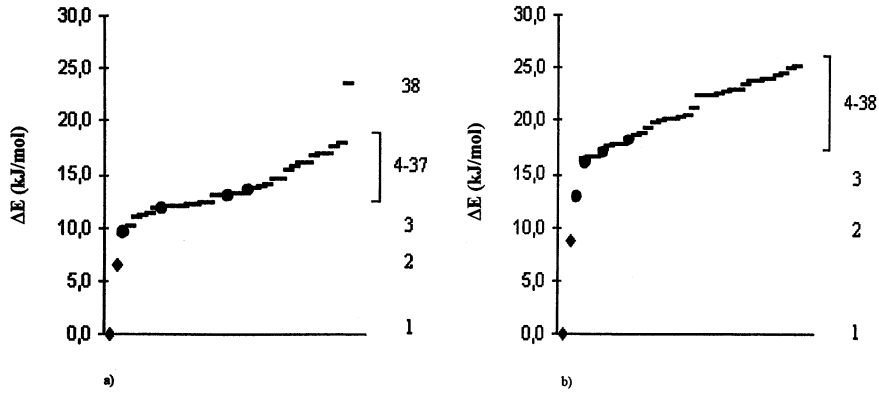

Fig. 2. Relative energies of the 38 local minima found in the a) HF and b) MP2 6-31G* potential energy surfaces of 3-amino-1-propanol with respect to the most stable structure.◆ conformers with an OH–N intramolecular hydrogen bond, ● conformers with an NH–O intramolecular hydrogen bond.

spectroscopic grade) as solvent and covering a concentration range from 2.5×10^{-3} M to 5.0×10^{-1} M.

Raman spectrum was obtained using a Spex 1403 double monochromator spectrometer (focal length 0.85 m, aperture $f/7.8$) equipped with holographic gratings with 1800 groove/mm (reference 1800-1SHD). The 514.5 nm Ar^+ laser, adjusted to provide 220 mW power at the sample, was used as excitation radiation. Detection was effected using a thermoelectrically cooled Hamamatsu R928 photomultiplier. The spectrum was recorded using increments of 1 cm^{-1} and integration times of 1 s.

Band intensities, from the matrix-isolation and Raman spectra, were obtained from the area of the observed peaks, subjected to previous deconvolution by using the peak fitting module of ORIGIN 4.0 [11].

A simulation of the Ar matrix and calculated HF 6-31G* spectra of isolated 3AP was performed by gaussian synthesis, from the experimental and ab initio frequencies and intensities, using the SYNSPEC programme [12].

The ab initio molecular orbital calculations were performed using the 6-31G* basis set [13] with the GAUSSIAN92 program package [14] running on a DEC ALPHA 7000 computer. Molecular geometries were fully optimised by the force gradient method using Berny's algorithm [15] and the standard convergence criteria for the geometry optimisation both at the Hartree-Fock and MP2 levels of theory. The HF 6-31G* ab initio calculated vibrational spectra were then used to help interpretation of the spectroscopic results, the calculated wavenumbers being scaled down in order to fit to the experimental values by using a single scale factor (0.89 [16]). Normal co-ordinates analysis was undertaken using the programs TRANSFORMER, BUILD-G and VIBRAT [17] which are interfaced with GAUSSIAN92.

3. Results and discussion

Relative energies of the 38 local minima found in the HF and MP2 potential energy surface of 3AP are shown graphically in Fig. 2. The three most stable conformers of the studied molecule are depicted in Fig. 3, and some calculated relevant data for these forms (relative energies, predicted population at room temperature assuming a Boltzmann distribution and selected structural data) are compared with the available experimental data in Table 1[1].

Considering the sum of Van der Waals radii of $(H + N) = 270$ pm and $(H + O) = 260$ pm [18], conformers I and II, with $r(OH–N) < 270$ pm, and conformer III, with $r(NH–O) < 260$ pm, are considered to be stabilised by an OH–N or NH–O

[1] Complete structural and energetic data for all the minima may be obtained from the corresponding author upon request.

intramolecular hydrogen bond, respectively, these interactions being the main factors responsible for their low energy.

From Fig. 2 it can be seen that there is a relatively large energy gap between the most stable form (I) and all the other conformers. This conformer is then predicted to be considerably more populated (MP2: 95.5%; HF: 78.8%) at room temperature than the remaining forms. The greater relative stability of this structure clearly shows that the intramolecular OH–N hydrogen bond it exhibits is considerably strong. The 2nd

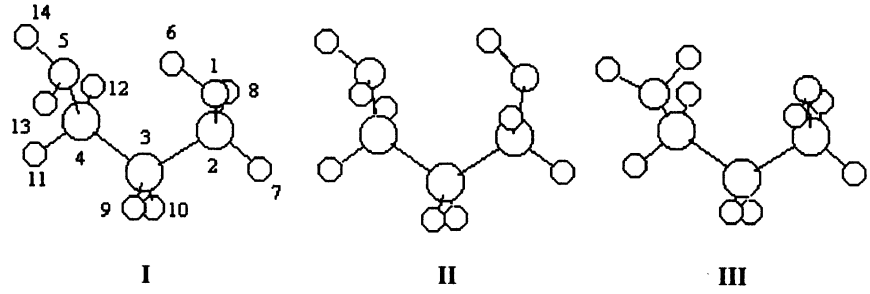

Fig. 3. Lowest energy conformers of 3-amino-1-propanol.

Table 1
Experimental and HF 6h31G*, MP2 6h31G* and DFT (B3Lyp 6h311++G(2d,2p)) calculated relevant data for the three most stable forms of 3-amino-1-propanol[a]

	Form I				Form II		Form III	
	Exp[b]	DFT[c]	HF	MP2	HF	MP2	HF	MP2
ΔE	0.00	0.00	0.00	0.00	6.57	8.82	9.55	12.77
p			78.8	95.5	5.6	2.7	1.7	0.6
p_i/p_I			1	1	0.07	0.03	0.02	0.01
Bond length								
CO	143	142.1	139.7	142.1	139.9	142.3	140.1	143.3
CN	148	147.8	146.3	147.6	146.0	147.3	145.5	146.8
OH	97	97.0	95.2	98.1	94.9	97.8	94.8	97.4
d(OH–N)	208	204	212	197	245	219	296	278
d(NH–O)			313	306	367	353	233	224
Dihedral								
H13N5C4C3	−66.5	−71.2	−68.7	−70.0	−63.3	−63.5	187.4	187.1
H14N5C4C3	173.5	170.5	173.1	173.7	178.5	180.4	68.7	70.6
N5C4C3C2	−68.9	−61.9	−60.5	−59.0	−45.3	−43.0	−71.7	−70.6
C4C3C2O1	76.6	67.7	70.2	69.4	−44.4	−40.9	59.9	58.1
C3C2O1H6	−42.0	−45.9	−52.8	−51.9	73.2	70.4	56.5	50.9
Charge								
H6			0.479	0.489	0.461	0.473	0.442	0.442
N			−0.877	−0.881	−0.870	−0.876	−0.862	−0.862

[a] Relative energies to the most stable conformer, ΔE, in kJ mol^{-1}; predicted populations, p (%), at room temperature, were calculated assuming a Boltzmann distribution (the total population of the remaining 35 conformers is predicted as p<14% and p<2% at the HF and MP2 levels of theory, respectively); bond lengths and distances in pm; dihedral angles in degrees; Mülliken atomic charges in units of electron ($1e^- = -1.6x10^{-19}C$).

[b] From [2].

[c] From [3].

lowest energy form, predicted to have an energy of 8.82 kJ mol^{-1} (HF: 6.57 kJ mol^{-1}) above the most stable conformer, has also an OH–N intramolecular H-bond, which is however considerably weaker than that present in the conformational ground state, as can be seen by comparing the distances between the atoms involved in this interaction in these two conformers (MP2: 197 pm versus 219 pm; HF: 212 pm versus 245 pm; see Table 1). The longer CN and OH bond distances, the larger absolute values for the atomic charges of H6 and N and the shorter CO bond length calculated for conformer I are also consistent with the existence in this form of a stronger H-bond interaction. On the other hand, form III, with an energy of ca. 12.77 kJ mol^{-1} (HF: 9.55 kJ mol^{-1}) above the most stable conformer, exhibits the much weaker NH–O intramolecular interaction. The calculations also predict the existence of three higher energy minima showing an intramolecular NH–O hydrogen bond (see Fig. 2).

It is worth to mention that the relative energies of the three lowest energy conformers calculated using the 6-31G* basis set are in good agreement with the previously reported values obtained by using the smaller 4-31G basis set or resulting from DFT calculations (4-31G [5]: $\Delta E_{II-I} = 8.91$, $\Delta E_{III-I} = 12.33$ kJ mol^{-1}; DFT [3]: $\Delta E_{II-I} = 8.95$, $\Delta E_{III-I} = 12.55$ kJ mol^{-1}). However, the lower level 4-31G theoretical calculations could only identify 33 of the 38 energy minima of 3AP.

In general, bond lengths and bond angles calculated at the different levels of theory do not show important differences, despite the MP2 calculations lead to slightly longer OH, CN and, specially CO bonds when compared with the Hartree-Fock values, thus matching closer the experimental values obtained by microwave spectroscopy [2]. Moreover, changes in these structural parameters with conformation were also found to be similar at the different levels of theory. Table 1 also compares the 6-31G* calculated values for the main dihedral angles of conformer I with those experimentally obtained [2]. These structural parameters are a good measure of the quality of the theoretical predictions, since they correspond to very flexible co-ordinates, strongly sensitive to intramolecular interactions. The 6-31G* values show a fairly good agreement with the experimental data, pointing to an adequate description by this basis set of the main intramolecular interactions that determine the preferred molecular conformations of 3AP. Since most of the geometric features that characterised the various conformers of 3AP were already well described elsewhere [5] they do not deserve here further treatment.

Table 2 summarises the 6-31G* calculated vibrational results obtained for the most populated conformational states (I, II and III) of isolated 3AP. The infrared spectrum of 3AP isolated in an Ar matrix is shown in Fig. 4. The absence of significant contribution of dimers (or higher order aggregates) to the observed spectra was checked by comparison with spectra obtained using low matrix/solute ratios (intensive mark bands of aggregated species appear at 3283, 775 and 767 cm^{-1}). The assignment of the observed bands is presented in Table 3 and a simulation of calculated and experimental (Ar matrix) spectra of 3AP, which allows an easier comparison between theoretical and experimental results, is shown in Fig. 5. As it could be anticipated, the vibrational bands owing to the most stable conformer I dominate the spectrum of 3AP in the low temperature matrix. The fact that the main observed bands occur as doublets (or triplets) could be ascribed to site splitting and demonstrates the existence of non-equivalent matrix sites. Some of the less intensive bands are as a result of conformers II and III. The comparison of the calculated and observed intensities of the bands ascribed to the νCN and νOH vibrations of the three conformers (these bands stay in a relatively clean spectral region and could be easily assigned to individual conformers) allows us to evaluate approximately the conformational composition of 3AP in the Ar matrix and to estimate the relative populations of forms I, II and III at the deposition temperature (298 K). The results show that, at this temperature, the relative populations of the three experimentally observed conformers are 1:0.021:0.003, which correspond to relative energies of $\Delta E_{II-I} = 9.54$ and $\Delta E_{III-I} = 14.23$ kJ mol^{-1}, respectively. These values compare fairly well with the corre-

Table 2
HF 6-31G* calculated relevant vibrational wavenumbers (ν) and absolute intensities (I^{ir}, infrared; I^{R}, Raman) for the most populated conformational states of 3-amino-1-propanol[a]

Approximate description[b]	Form I			Form II			Form III		
	ν	I^{ir}	I^{R}	ν	I^{ir}	I^{R}	ν	I^{ir}	I^{R}
νOH	3590	165.2	41.3	3632	70.2	38.3	3645	42.1	49.9
νNH_2as.	3388	2.1	80.0	3386	1.0	77.8	3410	7.0	54.3
νNH_2s.	3313	1.4	98.4	3313	0.7	98.6	3329	3.9	112.0
$\nu C2H_2$as.	2903	78.8	109.8	2911	86.0	91.8	2909	67.1	49.1
$\nu C4H_2$as.	2885	101.4	32.8	2903	53.4	57.3	2880	67.1	111.1
$\nu C3H_2$as.	2868	17.7	97.2	2878	41.5	57.5	2872	38.6	79.1
$\nu C3H_2$s.	2844	43.6	120.8	2836	66.0	80.9	2848	91.5	143.5
$\nu C4H_2$s.	2812	73.4	103.1	2812	70.7	84.1	2787	84.9	91.2
$\nu C2H_2$s.	2811	79.9	73.8	2860	48.0	146.9	2831	28.0	57.3
δNH2	1631	40.8	7.2	1634	42.5	7.2	1633	43.4	6.9
$\delta C2H_2$	1489	1.1	5.8	1484	0.3	11.5	1487	0.5	5.7
$\delta C4H_2$	1478	0.5	16.1	1491	1.4	8.2	1477	0.5	15.7
$\delta C3H_2$	1445	20.7	8.8	1452	5.8	13.3	1444	3.6	9.3
δCOH	1425	95.3	7.0	1371	21.8	6.8	1341	18.6	10.7
$\omega C4H_2$	1401	13.1	1.6	1411	25.4	1.8	1413	39.7	3.2
$\omega C2H_2$	1368	4.8	6.8	1390	47.6	4.5	1398	33.5	2.4
$\omega C3H_2$	1355	0.8	1.3	1357	1.5	1.7	1360	3.5	0.3
$twC4H_2$	1295	3.7	11.8	1379	11.2	8.1	1312	1.8	12.0
$twC3H_2$	1258	7.5	10.8	1268	4.8	18.4	1177	15.1	2.5
$twC2H_2$	1206	17.0	4.8	1194	11.1	0.7	1255	8.1	12.2
$\gamma C2H_2$	1145	5.4	3.1	978	16.3	2.6	934	15.3	3.9
νCO	1092	139.6	4.1	1088	77.9	4.6	1060	63.5	10.3
νCN	1054	28.5	7.1	1053	82.9	4.3	1048	44.3	1.9
γNH_2	1032	9.6	3.2	1138	2.9	2.4	1145	10.6	3.3
ωNH_2	943	30.5	5.7	866	121.5	4.9	902	52.4	3.2
νCcas.	920	7.8	6.4	932	16.1	6.3	1084	57.9	3.2
$\gamma C3H_2$	870	6.9	1.4	742	7.7	0.6	870	2.5	2.5
$\gamma C4H_2$	837	73.4	0.8	1009	2.7	4.7	846	73.8	2.5
νCCs.	774	4.3	11.8	797	11.1	12.5	771	5.9	12.0
τHOCC	605	183.6	2.8	504	141.7	1.8	239	158.9	2.5
δCCC	486	2.4	0.3	238	2.2	0.1	490	10.8	0.4
δOCC	369	12.6	1.1	563	25.0	0.4	307	10.7	0.8
δCCN	312	2.0	0.5	375	12.3	1.3	370	58.4	1.0
τCCNH	260	32.7	0.9	296	37.5	1.9	400	16.7	0.3
τOCCC	190	1.0	0.1	101	3.4	0.1	117	5.2	0.1
τCCCN	120	5.4	0.2	182	2.4	0.1	145	40.1	1.1

[a] Wavenumbers in cm^{-1}; wavenumbers were scaled by 0.89. Intensities in km mol^{-1}.
[b] Abbreviations: ν, stretching; δ, bending; γ, rocking; ω, wagging; τ, torsion; tw, twisting.

sponding MP2/6-31G* calculated values (8.82 and 12.77 kJ mol^{-1}).

The values of the OH stretching frequencies (main component band) for the conformational ground states in the Ar matrix for 2AE and 3AP, are 3555 cm^{-1} [1,18] and 3417 cm^{-1}, respectively, being consistent with the expected existence of a stronger intramolecular OH–N hydrogen bond in 3AP. It is also worth to mention that the vibrational calculations show the occurrence of an extensive coupling of co-ordinates in 3AP (see Table 3). This result can be correlated with the great torsional flexibility of this molecule and further reinforces the importance of intramolecular interactions in this system.

Fig. 6 shows the νOH region of the infrared spectra of 3AP in CCl_4 solution, at different concentrations. In these spectra, besides the typical broad band as a result of aggregates, bands as a result of monomeric species can be observed. The two low intensity bands appearing at the higher frequencies (3684 and 3639 cm^{-1}), can be assigned to monomeric forms III and II, respectively, while the band at 3396 cm^{-1}, which is superimposed with the band resulting from the aggregates, is ascribable to the conformational ground state (form I). These bands are observed at frequencies close to those of the corresponding bands in the spectra of the Ar-matrix isolated 3AP (3706, 3660 and 3417 cm^{-1}; see Table 4) though they are slightly red-shifted because of the higher effective polarity of the solvent.

The liquid phase infrared and Raman spectra of 3AP are shown in Fig. 7. The assignments of the observed bands in both spectra are presented in Table 4. Most of the bands of the spectra of the aggregates can be fairly well assigned taken as reference the calculated spectra of monomeric form III, indicating that this is the preferred conformation assumed by the monomeric units within the aggregates. As previously mentioned, the intramolecular NH–O hydrogen bond exhibited by this conformer (that is the lowest energy form having an intramolecular NH–O hydrogen bonding in isolated 3AP) makes the hydroxyl group more acidic and the amino group more basic and then activates both OH and NH_2 groups to the establishment of the intermolecular OH–N hydrogen bonding which is the dominant intermolecular interaction present in the aggregated species. The importance of this intermolecular hydrogen bonding in liquid 3AP is also reflected in the frequencies of the bands assigned to νOH, which strongly decrease when compared with those of the free monomeric species, and to δCOH and τHOCC, that increase when the OH group is involved in the intermolecular H-bonding [20]. These results are in agreement with the conclusions of our previous study in 2AE, where a conformation structurally similar to form III of 3AP was also found to be the preferred configuration assumed by the monomeric units within the aggregates, in the liquid phase [1].

On the other hand, very interestingly, in contrast with the results obtained for 2AE, there are spectroscopic evidences that some molecules adopting the conformational ground state of isolated 3AP-form I-are also present in the pure liquid. In particular, the infrared bands at 1224, 1149, 940 (this later also observed in the Raman spectrum) and 776 cm^{-1} assigned to the twC2H_2, γC2H_2, ωNH_2 and νCCs. vibrations, respectively, are ascribable to monomeric form I (see Table 3 for comparison with the frequencies of the corresponding bands in the matrix isolation spectrum

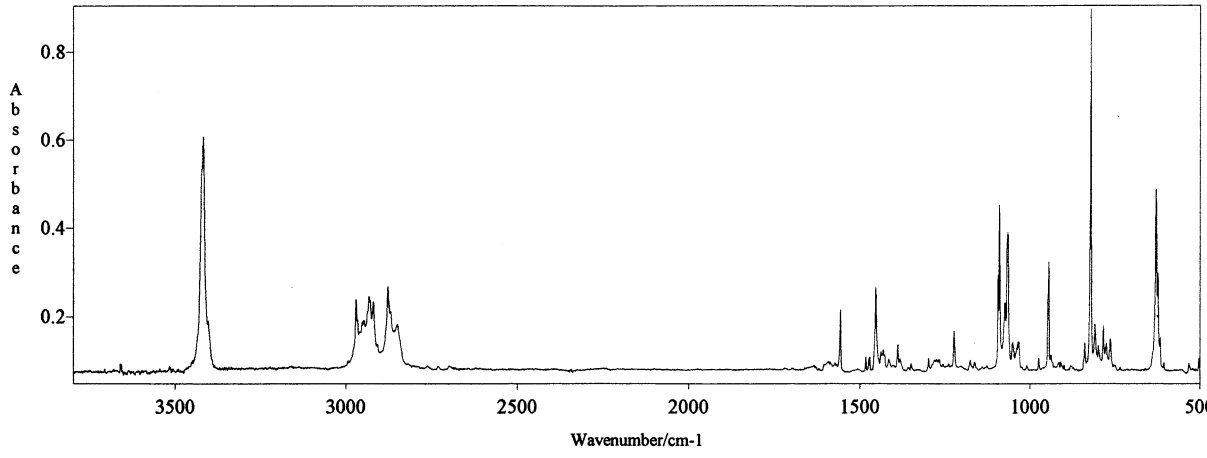

Fig. 4. Low temperature (14 K) infrared spectrum of 3-amino-1-propanol isolated in an Ar matrix (baseline corrected; water bands subtracted).

Table 3
Gas phase [19] and low temperature matrix isolation spectroscopy infrared vibrational spectra, HF 6–31G* calculated relevant infrared wavenumbers and intensities for the most populated conformational states of 3-aminopropanol and calculated potential energy distributions (PEDs) for the vibrations of the conformational ground state (I)[a]

Gas phase		MIS[b]		Calculated		PED[c]	Assignment[e]
ν	I	ν	I	ν	I		
3675	m	*3706*	*0.1*	*3645*	*0.9*		*νOH*III
3549	sh	*3660*	*2.0*	*3632*	*5.0*		*νOH*II
3494	m	3417	151.0	3590	165.2	νOH(99.9)	νOH
		3402[d]	16.2				
				3388	2.1	νNH_2as.(98.7)	νNH_2as.
				3313	1.4	νNH_2s.(98.6)	νNH_2s.
2939	vs	2971	41.6	2903	78.8	$\nu C2H_2$as.(63.9) + $\nu C2H_2$s.(33.1)	$\nu C2H_2$as.
		2967	*3.1*	*2911*	*6.1*		*νC2H*$_2$*as*.II
		2953	*1.5*	*2909*	*1.6*		*νC2H*$_2$*as*.III
		2947	*3.3*	*2903*	*3.8*		*νC4H2as*.II
		2937	*2.2*	*2880*	*1.4*		*νC4H2as*.III
2922	sh	2932	29.4	2885	101.4	$\nu C3H_2$as.(40.7) + $\nu C4H_2$as.(38.9) + $\nu C4H_2$s.(18.2)	$\nu C4H_2$as.
		2929	*6.2*	*2878*	*2.9*		*νC3H*$_2$*as*.II
2922	sh	2920	35.9	2868	17.7	$\nu C3H_2$as.(57.7) + $\nu C4H_2$as.(30.6)	$\nu C3H_2$as.
		2907	*3.4*	*2860*	*3.4*		*νC2H*$_2$*s*.II
2822	s	2877	37.7	2844	43.6	$\nu C3H_2$s.(90.6)	$\nu C3H_2$s.
		2873	*5.5*	*2836*	*4.7*		*νC3H*$_2$*s*.II
2822	s	2869	29.5	2812	73.4	$\nu C4H_2$s.(57.2) + $\nu C4H_2$as.(27.8)	$\nu C4H_2$s.
		2856	*4.6*	*2812*	*5.0*		*νC4H*$_2$*s*.II
2780	sh	2848	45.8	2811	79.9	$\nu C2H_2$s.(57.5) + $\nu C2H_2$as.(31.9)	$\nu C2H_2$s.
1624	m	1557	30.6	1631	40.8	δNH_2(79.1) + ωNH_2(19.4)	δNH_2
1487	sh	1482	16.6	1489	1.1	$\delta C2H_2$(66.7) + $\delta C4H_2$(29.0)	$\delta C2H_2$
1468	sh	1473	9.5	1478	0.5	$\delta C4H_2$(65.7) + $\delta C2H_2$(28.9)	$\delta C4H_2$
		1471[d]	3.5				
1435	m	1453	72.4	1425	95.3	$\omega C2H_2$(38.7) + δCOH(32.7)	δCOH
		1438	*5.4*	*1452*	*0.4*		*δC3H*$_2$ II
1435	m	1431	9.7	1445	20.7	$\delta C3H_2$(84.1)	$\delta C3H_2$
		1427[d]	7.8				
		1419	*1.6*	*1413*	*0.8*		*ωC4H*$_2$III
		1415	*0.9*	*1411*	*1.8*		*ωC4H*$_2$II
		1403	*0.5*	*1398*	*0.7*		*ωC2H*$_2$III
		1399	*0.6*	*1390*	*3.4*		*ωC2H*$_2$II
1390	m	1388	14.7	1401	13.1	$\omega C4H_2$(62.6)	$\omega C4H_2$
		1382	*0.5*	*1371*	*1.5*		*δCOH*II
1370	sh	1374	4.2	1368	4.8	$\omega C2H_2$(23.0) + $twC2H_2$(18.5) + δCOH(18.1) + $\omega C3H_2$(15.8)	$\omega C2H_2$
		1359	*0.2*	*1357*	*0.1*		*ωC3H*II
		1350	1.4	1355	0.8	$\omega C3H_2$(44.8) + $\omega C2H_2$(23.3) + $\omega C4H_2$(10.9)	$\omega C3H_2$
		1348[d]	2.8				
		1345	*0.1*	*1341*	*0.4*		*δCOH*III
1296	vw	1298	4.1	1295	3.7	$twC4H_2$(33.8) + γNH_2(25.4)	$twC4H_2$
		1288	*0.2*	*1279*	*0.8*		*twC4H*$_2$II
		1269	*1.0*	*1268*	*0.3*		*twC3H*$_2$II
1277	w	1266	3.6	1258	7.5	$twC3H_2$(31.3) + $twC4H_2$(28.0) + $twC2H_2$(13.3)	$twC3H_2$
		1239	*0.2*	*1255*	*0.2*		*twC2H*$_2$III
1237	w	1223	24.8	1206	17.0	$twC2H_2$(34.3) + δCOH(18.4) + $twC3H_2$(11.0)	$twC2H_2$
		1211	*0.6*	*1194*	*0.8*		*twC2H*$_2$II
1141	sh	1177	5.2	1145	5.4	$twC3H_2$(14.2) + $\gamma C2H_2$(12.1) + νCO(11.8) + $twC2H_2$(11.6) + γNH_2(10.0)	$\gamma C2H_2$
		1165	*0.1*	*1177*	*0.3*		*twC3H*$_2$III
		1159	*0.1*	*1145*	*0.2*		*γNH*$_2$III
		1127	*2.3*	*1138*	*0.2*		*γNH*$_2$II

Table 3 (continued)

Gas phase		MIS[b]		Calculated		PED[c]	Assignment[e]
ν	I	ν	I	ν	I		
1073	s	1095	44.3	1092	139.6	νCO(46.8)	νCO
		1092[d]	45.6				
		1088	*0.7*	*1084*	*1.2*		*νCCas*.III
		1078	*3.5*	*1088*	*5.5*		*νCO*II
		1075[d]	5.6				
1066	s	1069	43.7	1054	28.5	νCN(55.0)+νCCas.(25.3)	νCN
		1067[d]	62.7				
		1065[d]	67.7				
		1052	*1.7*	*1053*	*5.9*		*νCN*II
		1049	*0.7*	*1048*	*1.0*		*νCN*III
1054	sh	1037	15.7	1032	9.6	γNH_2(26.4)+νCO(15.4)+$\gamma C4H_2$(11.6)+tw$C3H_2$(10.1)	γNH_2
		1034[d]	23.1				
		1009	*1.6*	*1009*	*0.2*		*γC4H*$_2$II
		974	*1.2*	*978*	*1.1*		*γC2H*$_2$II
942	vw	947	24.7	943	30.5	ωNH_2(38.4)+tw$C4H_2$(13.2)+$\gamma C3H_2$(11.3)	ωNH_2
		945[d]	34.6				
		939	*0.8*	*932*	*1.1*		*νCCas*.II
		933	*0.7*	*934*	*0.3*		*γC2H*$_2$III
907	w	915	7.9	920	7.8	νCcas.(29.3)+νCN(27.6)	*νCCas*.
		910[d]	6.1				
		900	*0.2*	*902*	*1.1*		*ωNH*$_2$III
		882	*0.7*	*870*	*0.1*		*γC3H2*III
876	w	872	1.8	870	6.9	$\gamma C2H_2$(29.9)+$\gamma C3H_2$(15.6)+$\gamma C4H_2$(10.5)	$\gamma C3H_2$
		856	*0.1*	*846*	*1.6*		*γC4H*$_2$III
		839	*2.7*	*866*	*8.6*		*ωNH*$_2$II
810	sh	821	56.8	837	73.4	ωNH_2(39.2)+$\gamma C4H_2$(31.0)	$\gamma C4H_2$
		823[d]	32.9				
		809	*5.0*	*797*	*0.8*		*νCCs*.II
		807[d]	*1.6*				
		799[d]	*2.7*				
780	m	784	16.4	774	4.3	νCCs.(68.8)	νCCs.
		775[d]	3.3				
		765	*2.3*	*771*	*0.1*		*νCCs*.III
		763[d]	*0.2*				
		736	*0.3*	*742*	*0.5*		*γC3H*$_2$II
674	w	631	106.5	605	183.6	τHOCC(88.9)	τHOCC
		634[d]	54.9				
		625[d]	8.0				
		532	*5.5*	*563*	*1.8*		*δOCC*II
		502	*3.9*	*504*	*10.0*		*τHOCC*II
				486	2.4	δCCC (22.7)+δCCN(20.1)+$\gamma C3H_2$(20.0)+δOCC(18.5)	δCCC
				369	12.6	δOCC(44.1)+δCCN(21.0)	δOCC
				312	2.0	δCCN(26.4)+δCCC(23.4)+τOCCC(19.2)+τCCCN(11.0)	δCCN
				260	32.7	τCCNH (56.4)+τHOCC(19.1)+δCCC(15.2)	τCCNH
				190	1.0	τOCCC(50.4)+τCCCN(37.4)	τOCCC
				120	5.4	τCCCN(32.7)+τHOCC(31.5)+τOCCC(28.4)	τCCCN

[a] Wavenumbers in cm^{-1}; calculated wavenumbers were scaled by 0.89. MIS experimental intensities are normalised integrated intensities (I_i^{obs}) obtained using the formula $I_i = I_i^{obs} \times \Sigma I_i^{cal}/\Sigma I_i^{obs}$ (where ΣI_i^{cal}, sum of the calculated intensities; ΣI_i^{obs}, sum of the observed intensities; i, observed band); integrated intensities were measured after deconvolution. Calculated intensities (Km mol^{-1}) are presented as relative intensities to form **I** taking into consideration the populations of the conformational states. Data related to forms **II** and **III** are given in italic.

[b] Infrared in Ar matrix.

[c] Only PED values larger than 10% are shown in this table.

[d] Site splitting.

[e] Abbreviations: ν, stretching; δ, bending; γ, rocking; ω, wagging; τ, torsion; tw, twisting.

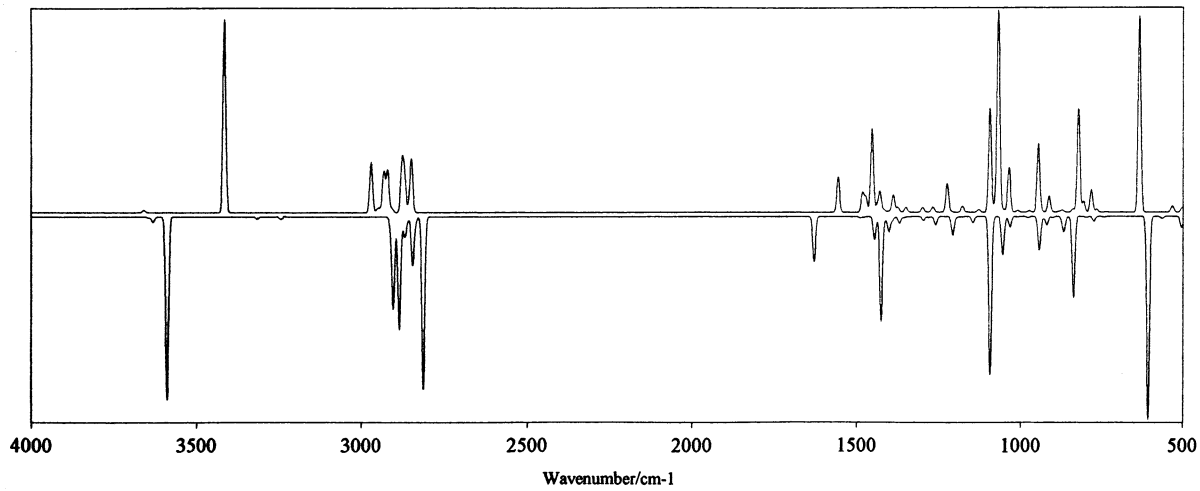

Fig. 5. Simulation of the Ar matrix (lower) and calculated HF 6-31G* (upper) spectra of 3-amino-1-propanol in the 4000-500 cm^{-1} spectral region, obtained by gaussian synthesis from the experimental and ab initio frequencies and intensities (constant half band width assumed). Calculated wavenumbers were scaled by 0.89. Calculated intensities presented as relative intensities to form **I** (considering the predicted populations of the conformational states); experimental intensities are normalised intensities [I_i^{obs} (norm)] obtained from the area of each observed peak, subjected to previous deconvolution (I_i^{obs}), by using the formula I_i^{obs} (norm) = $I_i^{obs} \times \Sigma I_i^{cal}/\Sigma I_i^{obs}$ (where ΣI_i^{cal}, sum of the calculated intensities; ΣI_i^{obs}, sum of the observed intensities; i, observed band). When site splitting occurs, experimental wavenumbers correspond to weighted averages [$\upsilon^{obs} = \Sigma \upsilon^{iobs} \times I^{iobs}(norm)/\Sigma I_i^{obs}(norm)$] and intensities are the sum of the intensities of all component bands. The total intensity of each spectrum was normalised to unit.

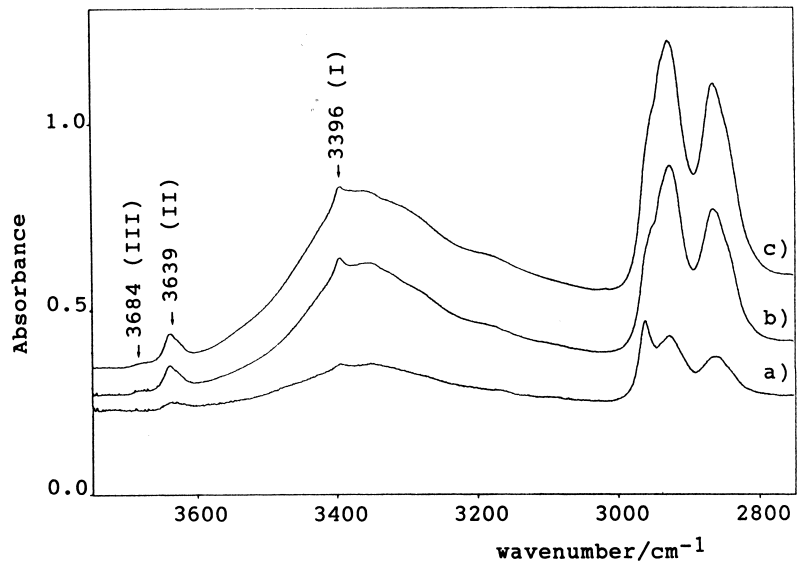

Fig. 6. Infrared spectra (3750–2750 cm^{-1} region) of 3-amino-1-propanol in CCl_4 solution, at room temperature. Concentrations are: (a) 15 mM; (b) 100 mM; and (c) 500 mM.

Table 4
Comparison of the infrared and Raman spectra of pure liquid with the calculated spectra of form III (see text)[a]

Infrared		Raman		Calculated			PED[b]	Assignment[d]
ν	I^{ir}	ν	I^{R}	ν	I^{ir}	I^{R}		
3353	vs	3368	25.0	3410	7.0	54.3	νNH_2as.(97.4)	νNH_2as.
3290	vs	3310	80.4	3329	3.9	112.0	νNH_2s.(97.7)	νNH_2s.
3193	vs	3196	40.0	3645[c]	42.1	49.9	νOH(100)	νOH
		2958	37.5	2909	75.5	49.1	$\nu C2H_2$as.(68.6)+$\nu C2H_2$s.(24.6)	$\nu C2H_2$as.
2935	vs	2918	130.0	2880	67.1	111.1	$\nu C4H_2$as.(58.2)+$\nu C4H_2$s.(36.4)	$\nu C4H_2$as.
		2911	87.0	2872	38.6	79.1	$\nu C3H_2$as.(91.9)	$\nu C3H_2$as.
		2878	84.4	2848	91.5	143.5	$\nu C3H_2$s.(49.4)+$\nu C2H_2$s.(36.3)+$\nu C2H_2$as.(10.4)	$\nu C3H_2$s.
2872	vs	2858	28.2	2831	28.0	57.3	$\nu C3H_2$s.(44.6)+$\nu C2H_2$s.(37.4)+$\nu C2H_2$as.(15.8)	$\nu C2H_2$s.
		2840	5.1	2787	84.9	91.2	$\nu C4H_2$s.(60.7)+$\nu C4H_2$as.(37.7)	$\nu C4H_2$s.
1599	s	1615	9.2	1633	43.4	6.9	δNH_2(78.4)+ωNH_2(20.1)	δNH_2
1475	m	1486	16.2	1487	0.5	5.7	$\delta C2H_2$(67.0)+$\delta C4H_2$(29.3)	$\delta C2H_2$
		1480	17.4	1477	0.5	15.7	$\delta C4H_2$(66.0)+$\delta C2H_2$(28.6)	$\delta C4H_2$
1430	m	1450	16.3	1444	3.6	9.3	$\delta C3H_2$(92.6)	$\delta C3H_2$
		1410	0.8	1413	39.7	3.2	$\omega C4H_2$(51.5)+$\omega C2H_2$(17.5)	$\omega C4H_2$
1393	sh			1398	33.5	2.4	$\omega C2H_2$(47.0)+νCcas.(12.9)	$\omega C2H_2$
1374	m	1378	16.8	1360	3.5	0.3	$\omega C3H_2$(48.3)+$\omega C2H_2$(16.1)+$\omega C4H_2$(10.1)	$\omega C3H_2$
1353	m			1341[c]	18.6	10.7	δCOH (34.5)+$twC2H_2$(16.1)+$\omega C3H_2$(10.1)	δCOH
1328	m	1308	43.0	1312	1.8	12.0	$twC4H_2$(36.0)+γNH_2(23.3)	$twC4H_2$
1240	vw	1246	8.3	1255	8.1	12.2	$twC2H_2$(36.3)+$twC3H_2$(27.7)+$twC4H_2$(13.1)	$twC2H_2$
1211	vw	1168	2.6	1177	15.1	2.5	$twC3H_2$(25.8)+$\gamma C4H_2$(15.4)+γNH_2(12.5)	$twC3H_2$
1108	sh	1118	13.1	1145	10.6	3.3	$twC4H_2$(24.4)+γNH_2(17.3)+$twC2H_2$(12.6)	γNH_2
1073	s	1084	24.5	1084	57.9	3.2	νCO(28.9)+νCCas.(26.3)+νCN(11.3)	νCCas.
1054	s	1068	20.5	1060[c]	63.5	10.3	νCO(38.7)+νCN(22.0)	νCO
1021	sh	1034	13.5	1048	44.3	1.9	δCOH(20.7)+νCN(15.7)+$\gamma C2H_2$(10.8)	νCN
965	m	992	13.3	934	15.3	3.9	νCcas.(23.8)+νCN(16.6)+$\gamma C2H_2$(12.9)+ωNH_2(12.1)	$\gamma C2H_2$
910	m	922	27.3	902	52.4	3.2	ωNH_2(37.6)+$\gamma C2H_2$(14.7)+νCN(12.6)	ωNH_2
859	w	870	16.7	870	2.5	2.5	$\gamma C4H_2$(30.7)+$\gamma C3H_2$(27.1)+γNH_2(13.1)	$\gamma C3H_2$
823	w	844	20.3	846	73.8	2.5	ωNH_2(33.4)+$\gamma C2H_2$(21.9)+$\gamma C4H_2$(17.1)	$\gamma C4H_2$
760	w	808	9.2	771	5.9	12.0	νCCs.(65.3)+$\gamma C3H_2$(10.0)	νCCs
530	w	536	12.7	239[c]	158.9	2.5	τCCNH(36.3)+τHOCC(34.8)+δCCC(18.1)	τHOCC
				490	10.8	0.4	δOCC (25.7)+$\gamma C3H_2$(21.8)+δCCC(20.0)+δCCN(13.8)	δCCC
		424	19.2	400	16.7	0.3	τCCNH(44.3)+τHOCC(40.1)	τCCNH
		390	15.6	370	58.4	1.0	δCCN(50.2)+δOCC(11.6)	δCCN
		292	10.4	307	10.7	0.8	δOCC(27.2)+δCCC(26.0)+τCCCN(12.8)	δOCC
				145	40.1	1.1	τCCCN(29.7)τOCCC(22.9)+τCCNH(22.9)+τHOCC(21.2)	τCCCN
				117	5.2	0.1	τOCCC(43.0)+τCCCN(31.9)+τCCNH(13.7)	τOCCC

[a] Wavenumbers in cm^{-1}; calculated wavenumbers were scaled by 0.89. Intensities in km mol^{-1}; infrared experimental intensities (I^{ir}) presented as qualitative relative intensities; Raman experimental intensities are normalised intensities (I^{R}) obtained from the area of each observed peak, subjected to previous deconvolution (I_i^{obs}), by using the formula $I^{R} = I_i{}^{obs} \times \Sigma I_i^{cal}/\Sigma I_i^{obs}$ (where ΣI_i^{cal} = sum of the calculated intensities, ΣI_i^{obs} = sum of the observed intensities, i = observed band).

[b] Only Potential Energy Distribution (PED) values larger than 10% are shown in this table.

[c] As it is usually observed [20], when the OH group participates in H-bonding, the wavenumbers of νOH and νCO decrease while those of δCOH, τHOCC increase relatively to the isolated molecule situation.

[d] Abbreviations: ν, stretching; δ, bending; γ, rocking; ω, wagging; τ, torsion; tw, twisting.

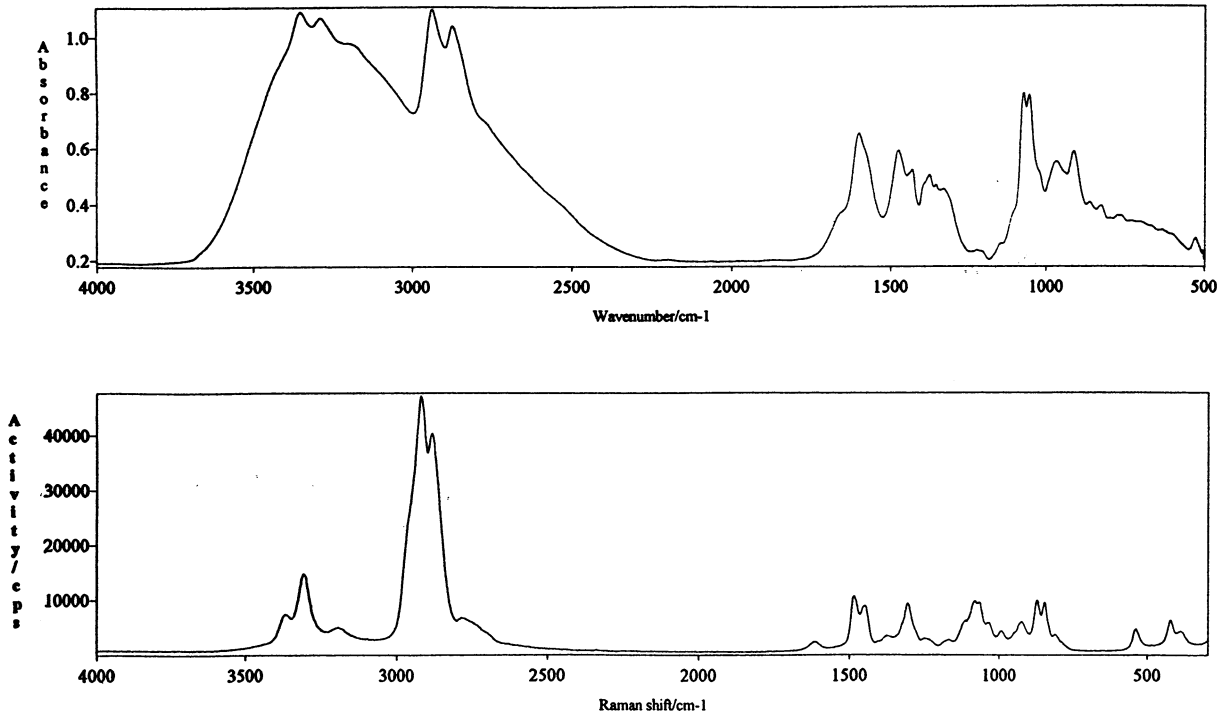

Fig. 7. Liquid phase infrared (upper) and Raman (bottom) spectra of 3-amino-1-propanol (room temperature).

and with the calculated frequencies for this form). In addition, the dependence with temperature of the infrared bands at 1328 and 1054 cm^{-1} (ascribed to $twC4H_2$ and νCO of the aggregates), also indicates that these bands must have a partial contribution from vibrational modes of monomeric form I (in particular $\omega C3H_2$ and νCN).

The different behavior of 2AE and 3AP with respect to the presence of monomeric molecules adopting the conformation I in the liquid phase can be correlated with the fact that the intramolecular OH–N hydrogen bond in the conformational ground state of isolated 3AP is much stronger than in isolated 2AE. Indeed, besides the lower observed νOH frequency for 3AP already mentioned, the calculations also show that form I of 3AP has a longer OH bond length and a shorter N–HO distance when compared with the corresponding conformer of 2AE (Table 5). Furthermore, a previous theoretical work on aminoalcohols carried out using the 4–31G basis set also indicated that the strength of the intramolecular OH–N interaction in linear aminoalcohols should increase with ring size [5].

The strong intramolecular OH–N interaction in 3AP reduces the association tendency in the pure liquid and some monomers of form I are still present in this phase. An increase of temperature leads to an increase of the relative intensities of the bands assigned to this form (Fig. 8), since the ratio between the free and H-bonded species shall increase with temperature (the overall process of complexation is exoenergetic) [21]. A detailed quantitative analysis of this association process,

Table 5
HF 6-31G* calculated OH bond lengths, N–HO distances for the conformational ground states of 3-amino-1-propanol and 2-aminoethanol for the isolated molecule situation[a]

	r(OH)	r(N–HO)
2-aminoethanol	95.03	232
3-amino-1-propanol	95.15	212

[a] Distances in pm.

which is complicated by the change of conformation upon complexation, deserves further attention and studies are actually running in our laboratory to address this question.

Acknowledgements

The authors acknowledge Dr João Cecílio for his technical help. This work was held within the PRAXIS XXI (QUI/2/2.1/412/94) research programme that is also partially funded by FEDER. Constança Cacela acknowledges the Ph.D. grant (GGPXXI/BD/3873/96) from Fundação para a Ciência e Tecnologia, Lisbon.

References

[1] C.F.C.P. Silva, M.L.T.S. Duarte, R. Fausto, J. Mol. Struct. 482–483 (1999) 591.
[2] M.A. McMahan, S.D. Sharma, R.F. Curl Jr, J. Mol. Spectrosc. 75 (1979) 220.
[3] M. Przeslawska, S.M. Melikowa, P. Lipkowski, A. Koll, Vibrat. Spectrosc. 20 (1999) 69–83.
[4] A.-M. Kelterer, M. Ramek, J. Mol. Struct. (Theochem) 232 (1991) 189.
[5] A.-M. Kelterer, M. Flock, M. Ramek, J. Mol. Struct. (Theochem) 276 (1992) 61.
[6] M. Ramek, M. Flock, A.-M. Kelterer, V.K.W. Cheng, J. Mol. Struct. (Theochem), 267 (1992) 61.
[7] S.T. Mulla, C.I. Jose, J. Chem. Soc. Faraday Trans. I 82 (1986) 707.
[8] P.J. Krueger, H.D. Meettee, Can. J. Chem. 43 (1965) 2970.
[9] Y.-P. Chang, T.-M. su, T.-W. Li, I. Chao, J. Phys. Chem. A101 (1997) 6107.
[10] R.L. Sutton, Chem. Britain 27 (1991) 432.
[11] Microcal software, Microcal origin (Version 4.0), copyright© 1991–1995.
[12] K.K. Irikura, SYNSPEC, Physical and Chemical Properties Division National Institute of Standards and Technology, Gaithersburg, MD, 1995.
[13] W.J. Hehre, R. Ditchefield, J.A. Pople, J. Chem. Phys. 56 (1972) 2257.
[14] M.J. Frisch, G.W. Trucks, H.B. Schelegel, P.M.W. Gill, B.G. Johson, M.W. Wong, J.B. Foresman, M.A. Robb, M. Head-Gordon, E.S. Replogle, R. Gomperts, J.L. Andres, K. Raghavachari, J.S. Binkley, C. Gonzalez, R.L. Martin, D.J. Defrees, J. Baker, J.J.P. Stewart, J.A. Pople, GAUSSIAN92/DFT (Revision G.2), Gaussian, Pittsburg, PA, 1993.
[15] H.B. Schlegel, Ph.D. Thesis, Queen's University, Kingston, Ontario, Canada, 1975.
[16] D.J. Defrees, A.D. McLean, J.Chem.Phys. 82 (1985) 333.
[17] M.D.G. Faria, R. Fausto, TRANSFORMER, BUILD-G and VIBRAT (version 1.0), Departamento de Química, Universidade de Coimbra, Portugal, 1990.
[18] M. Räsänen, A. Aspiala, L. Homanen, J. Murto, J. Mol. Struct 96 (1982) 81.
[19] EPA Vapor Phase Library (CAS 156-87-6), Galactic Industries, Salem, NH, 1994.
[20] R. Fausto, J. Mol. Struct. 377 (1996) 181.
[21] G.S.F. D'Alva Torres, C. Pouchan, J.J.C. Teixeira-Dias, R. Fausto, Spectrosc. Lett. 26 (1993) 913.